

MICROMECHANISMS OF CLEAVAGE FRACTURE IN FERRITIC STEELS

P. Bowen⁺, R.J. Condor⁺ and J.F. Knott^x

Many recent studies have established that in general the micromechanism of cleavage fracture is controlled by a combination of critical tensile stress, and large microcrack nuclei such as carbides or inclusions. These observations have been consistent with the use of a modified Griffith relationship. This paper reviews such studies and considers a controlled experiment in mild steel where both the microcrack nuclei and grain sizes have been held constant yet large differences in both microscopic cleavage fracture stress and fracture toughness are observed.

INTRODUCTION

Many recent studies have concluded from the temperature independence of the microscopic cleavage fracture stress, σ_F^* , that is often observed for example, Bowen et al. (1), Curry and Knott (2), that the mechanism of cleavage fracture in ferritic steels is growth controlled. Moreover, good agreement has been shown in many cases with a modified Griffith criterion based on σ_F^* and the sizes of the coarsest observed second phase particles (equated to the sizes of the microcrack nuclei), see for example Figure 1. Studies on weld-metals McRobie and Knott (3), Bowen et al. (4), have also proven unambiguously the role of peak tensile stress and have confirmed the importance of large microcrack nuclei (silicate inclusions), Figure 2. Some qualitative success has also been achieved in terms of statistical modelling of sharp-crack fracture toughness by considering the sampling of microcrack nuclei by high tensile stresses ahead of a sharp crack. The weld-metal studies have indicated that such models must incorporate not only the sizes of microcrack nuclei but also their location since the most potent nuclei are found in large ferrite grains (3), Figure 3. Indeed, previous studies have also demonstrated improvements in σ_F^* even when a constant population of large microcrack nuclei has been maintained, Hodgson and Tetelman (5).

⁺ School of Metallurgy and Materials/IRC in Materials for High Performance Applications, University of Birmingham.

^x Department of Materials Science and Metallurgy, University of Cambridge.

This present study indicates effects of unpinned dislocations on σ_F^* in mild steel which cannot be accounted for by using existing micromodels of fracture toughness behaviour.

EXPERIMENTAL

The material used was mild steel, of nominal composition 0.07 wt.% C, 0.50 wt.% Mn. Controlled heat-treatments were performed under vacuum and in all cases involved austenitising at 980°C for 24 hrs. followed by furnace cooling to 700°C and holding for 1 hr. Testpieces were then either: quenched rapidly into iced-brine and then transferred and held at liquid nitrogen prior to testing (IBQ); or furnace cooled to room temperature and aged subsequently for 1 hr. at 140°C (FC and aged). Additionally, some quenched testpieces were also aged at 140°C prior to testing (IBQ and aged). SEN band testpieces (of width 12.7 mm and thickness 12.7 mm) were used for both σ_F^* testing (blunt-notch testpieces of notch root radius 0.25 mm, ground in prior to heat-treatment) and fracture toughness, K_{IC} , testing (pre-cracks were introduced in accordance with BS5447: 1977 prior to heat-treatment). Tensile tests were performed on Hounsfield number 13 testpieces. Fracture toughness tests were carried out in accordance with BS5762: 1979, and resulted in unstable (or critical) crack opening displacement, $\delta_u(\delta_c)$ values. Careful metallographic and fractographic studies were also performed, Condor (6).

RESULTS

The heat-treatment schedules have resulted in a constant average ferrite grain size of 53 μm , an average cleavage facet size of 60 μm , and grain boundary carbide sizes of $1.66 \pm 0.95 \mu\text{m}$ IBQ, $1.41 \pm 0.54 \mu\text{m}$ IBQ and aged, and $1.80 \pm 0.84 \mu\text{m}$ FC and aged. The coarsest observed carbide size was measured as 4.2 μm . In all cases the microstructure consisted of ferrite grains together with regions of localised pearlite and grain boundary carbides. Often grain-boundary carbides were observed in close proximity to pearlite colonies, see also Mintz and Campbell (7). Despite careful transmission electron microscopy (TEM) studies no additional precipitation could be detected for the IBQ and aged condition. Local regions of microvoid coalescence in a cleavage matrix were observed on fracture surfaces and their average area fraction measured at 3.05% is consistent with the average area fraction of pearlite measured on metallographic sections as 3.14%.

Yield stress versus test temperature plots are shown in Figure 4. Most importantly a yield drop is observed in all cases for the IBQ and aged condition but absent for the IBQ condition. This confirms that unpinned dislocations are produced on quenching and retained by refrigeration at -196°C for this latter condition. It is of interest to note that the yield stress measured in the FC and aged condition is closely similar to that for the IBQ condition, whereas for the IBQ condition ageing approximately doubles its yield stress. Figure 5 shows the values of σ_F^* obtained for these conditions, (σ_F^* is defined as the maximum tensile stress present ahead of the notch at failure, see (1)). Average values calculated are 900 MPa (FC and aged), 1130 MPa (IBQ) and 1370 MPa (IBQ and aged). Values of σ_F^* for the IBQ condition obtained at -100 and -80°C are out of range of the analysis but an upper bound value is calculated at -100°C as 1180 MPa (the invalid values shown in Figure 5 are necessarily lower bound

values). Critical or unstable crack opening displacement values, δ , are shown as a function of test temperature in Figure 6. Some scatter is observed, but the FC and aged condition exhibits the lowest transition temperature and highest toughness. The highest transition temperature and lowest toughness is exhibited by the IBQ and aged condition.

DISCUSSION

Several results in the present work are of note. First, the two fold increase in yield stress on ageing the IBQ condition is unexpected. Since the grain size is constant, this is attributed to a decreased effective slip-band length for this condition due to carbon atmospheres or carbide clusters produced on ageing but it is disappointing that this could not be confirmed by TEM. Second, the unpinned dislocations present in the IBQ condition have increased the value of σ_F^* compared with the FC and aged condition (of similar yield stress). Most importantly, since the distributions of microcrack nuclei (coarse grain-boundary carbides) and ferrite grain sizes are constant for all three conditions then subtle effects of dislocation mobility and effective slip-band lengths are suggested. Support for this latter concept has been seen previously where a fine distribution of carbides seems to have shielded the coarser carbides and promoted higher values of σ_F^* (5).

It is, however, intriguing that present day models, for example Bowen et al. (8) of fracture toughness would predict that the IBQ condition to be the toughest followed by the FC and aged condition and finally the IBQ and aged condition. Such predictions are based on the stress intensification required to raise the yield stress to the microscopic cleavage fracture stress for a constant microstructurally significant distance and have been successful particularly in predicting upper temperatures for possible cleavage fracture. The results shown in Figure 6 indicate clearly that the FC and aged condition possesses the best toughness. Moreover, at the temperatures of -100 and -80°C , even if lower bound values of σ_F^* shown in Figure 5 for the IBQ condition are used, this is insufficient to predict lower toughness for this condition compared with the FC and aged condition. Therefore, it is concluded that unpinned dislocations (IBQ condition) can promote increased cleavage fracture resistance in blunt notch testpieces (higher σ_F^* values) but no such improvements are observed in sharp-crack testpieces where lower toughness values are obtained (relative to the FC and aged condition). Further work is required to explain the physical basis for such unexpected results, but the present work illustrates the difficulties inherent to formulating quantitative micromodels of sharp-crack fracture toughness in ferritic steels.

CONCLUSIONS

1. Although the micromechanism of cleavage fracture appears to be controlled in general by a combination of peak tensile stress and large microcrack nuclei, marked effects due to dislocation mobility can be observed in ferritic steels when coarse microstructural parameters are held constant.

- Improvements in cleavage fracture resistance (σ_F^* values) that can be attributed to unpinned dislocations in blunt notch tests do not result in increased toughness in sharp-crack tests for the same microstructural condition.

ACKNOWLEDGEMENTS

Thanks are due to Professor D. Hull FRS, University of Cambridge and Professor I.R. Harris, University of Birmingham for the provision of research facilities during the course of this work.

REFERENCES

- Bowen, P., Druce, S.G. and Knott, J.F., Acta Metall., Vol. 34, No. 67, 1986, pp. 1121-1131.
- Curry, D.A. and Knott, J.F., Met. Sci., Vol. 10, 1976, pp. 1-10.
- McRobie, D.E. and Knott, J.F., Met. Sci., Vol. 17, 1983, pp. 45-54.
- Bowen, P., Ellis, M.B.D., Strangwood, M. and Knott, J.F., ECF 6, Vol. 3, 1986, pp. 1751-1762.
- Hodgson, D.E. and Tetelman, A.S., J. Metals, Vol. 21, 1969, pp. A132.
- Condor, R.J. Unpublished Work, 1990.
- Mintz, B. and Campbell, P., Met. Sci. and Tech., Vol. 5, 1989, pp. 2.
- Bowen, P., Druce, S.G. and Knott, J.F. Acta Metall., Vol. 35, No. 7, 1987, pp. 1735-1746.

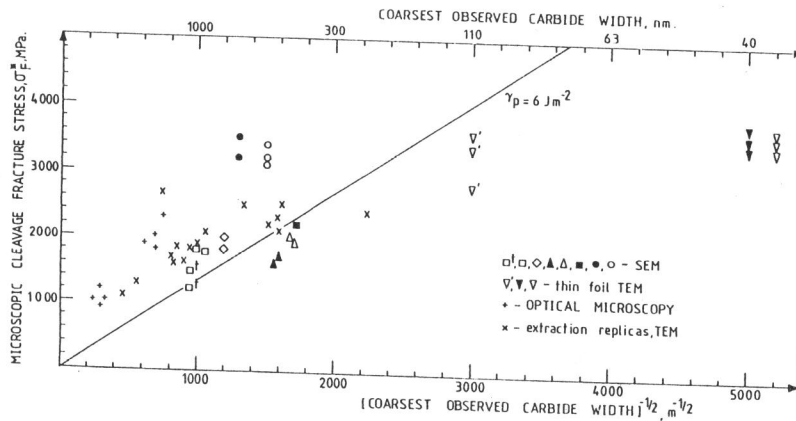


Figure 1 σ_F^* versus (carbide width)^{-1/2}

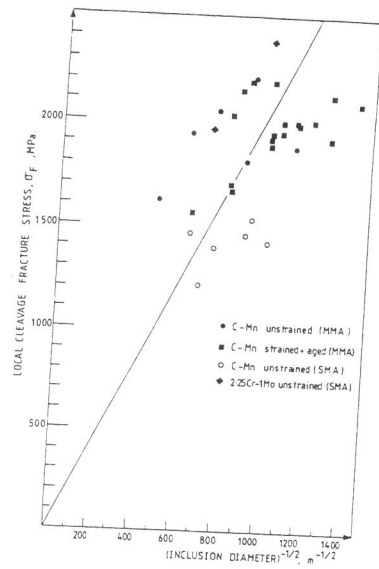


Figure 2 Local fracture stress versus (inclusion diameter)^{-1/2}

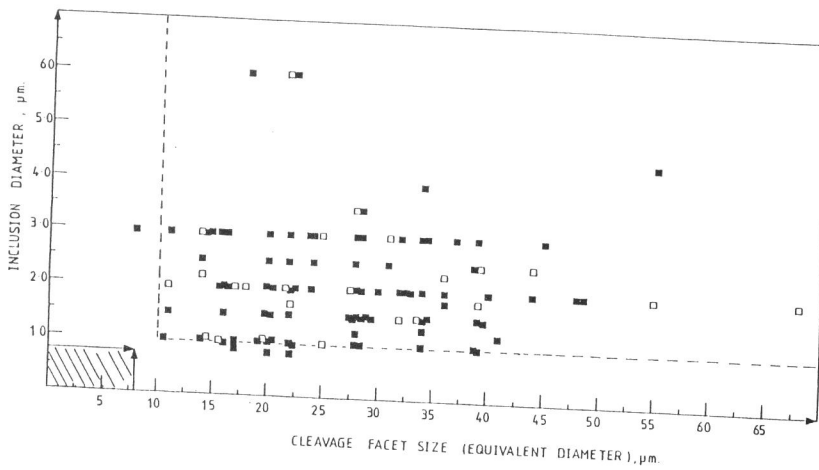


Figure 3 Local cleavage initiation sites. The hatched area defines limits of mean inclusion and ferrite grain sizes

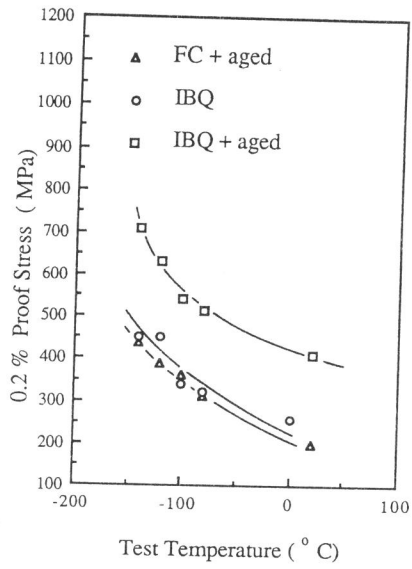


Figure 4 Yield stress versus test temperature

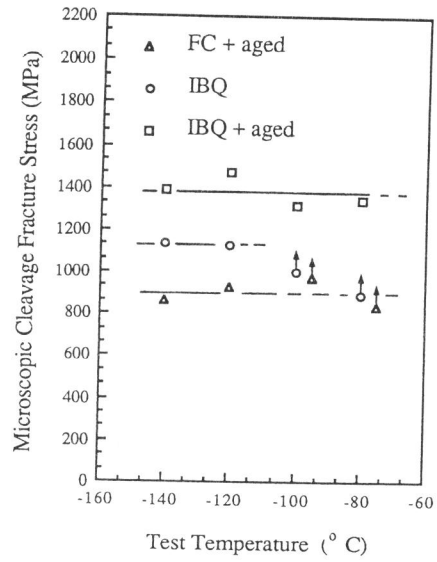


Figure 5 Microscopic cleavage fracture stress versus test temperature

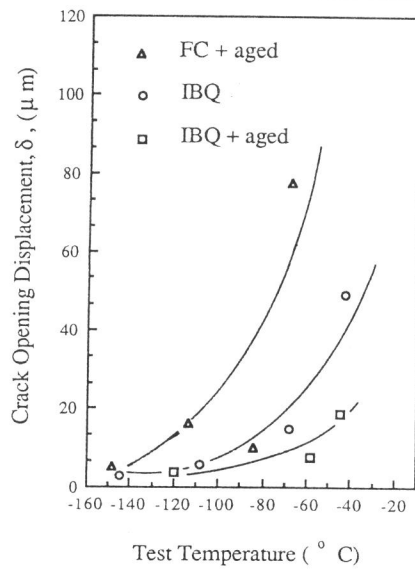


Figure 6 Crack opening displacement versus test temperature.